Eur. J. Mineral.
2007, **19**, 255–265

Vihorlatite, $Bi_{24}Se_{17}Te_4$, a new mineral of the tetradymite group from Vihorlat Mts., Slovakia

ROMAN SKÁLA[1,*], PETR ONDRUŠ[2], FRANTIŠEK VESELOVKÝ[2], ZDENĚK TÁBORSKÝ[2], and RUDOLF ĎUĎA[3]

[1]Institute of Geology, Academy of Sciences of the Czech Republic, Rozvojová 269, 16500 Praha 6, Czech Republic
*Corresponding author, e-mail: skala@gli.cas.cz
[2]Czech Geological Survey, Klárov 3/131, 11821 Praha 1, Czech Republic
[3]Museum of Eastern Slovakia, Hrnčiarská 7, 04001 Košice, Slovak Republic

Abstract: Vihorlatite, ideally $Bi_{24}Se_{17}Te_4$, is a new mineral species found in the region of volcanic Vihorlat Mountains in eastern Slovakia. It occurs in quartz-opal veinlets or secondary quartzites as anhedral to subhedral grains flattened parallel to (0001) up to 8 mm in diameter or aggregates thereof. The mineral is steel grey in colour and shows a metallic lustre. It displays a perfect cleavage along (0001) and shows deformation lamellae in mechanically bent crystals. In reflected light, it is white with a yellow tint, bireflectance is not perceptible in air, and anisotropy is moderate varying from light yellow-grey to dark grey. Maximum and minimum values of reflectance measured in air for 470, 546, 589 and 650 nm are (R_{max}/R_{min} in %): 52.9/49.9, 54.5/50.6, 54.6/51, 54.7/51.2. Vickers micro-hardness (VHN_{50} in kg/mm^2) varies in the range 49.2 – 91.7 with mean value of 65.9. Average chemical composition (in wt. %) Bi 71.5, Se 21.4, Te 8.1, S 0.8, Au 0.01, Ag 0.01, Sb 0.04, total 101.86, results in an empirical formula $Bi_{21.9}Se_{17.4}Te_{4.1}S_{1.6}$. The mineral is trigonal, with space group $P\bar{3}m1$. The unit-cell dimensions refined from powder data are a = 4.2797(9) Å and c = 87.01(2) Å with c/a = 20.332(6) and V = 1380.2(6) Å^3. For Z = 1, the calculated density is D_x = 7.850(3) g/cm^3, measured density D_m = 8.0(2) g/cm^3. The five strongest diffraction lines are [d (Å), I/I_0, (hkl)]: 4.55, 55.4, (0.0.19); 3.116, 100, (1.0.15); 2.282, 75.5, (0.1.30); 1.934, 42.8, (1.1.19) (0.0.45); 1.767, 31.5, (0.2.15). The crystal structure of vihorlatite is derived from that of Bi_8Se_7 archetype. Vihorlatite belongs to the tetradymite group.

Key-words: vihorlatite, new mineral, tetradymite group, crystal structure, Vihorlat Mts., Slovakia.

Introduction

Vihorlatite – together with other Bi–Se–Te(±S) phases, including the relatively recently described phase telluronevskite (Řídkošil *et al.*, 2001) – was discovered during a regional geological and mining prospection in the Vihorlat Mountains of Slovakia. It was found at a site located approximately 8 km SSE of the municipality Snina and ~ 20 km E of the town Humenné (Fig. 1; Sopková, 1977; Ďuďa, 1985). The new mineral and its name have been approved by CNMMN IMA (No. 88-047c). The mineral name is derived from the locality. The type material is deposited in the mineral collection of the National Museum in Prague, Czech Republic, under the catalogue number P1N 84444 and the acquisition number P1p 5/89.

Vihorlatite is a new member of the tetradymite group which includes minerals of layered trigonal bismuth(±Ag, Pb)-chalcogenides. A general crystallochemical formula of these minerals, reflecting the basic building blocks, consisting of individual planar atomic layers stacked perpendicular to **c**-axis, is $(Bi_2)_p(Bi_2X_3)_q$ or $(X_2)_p(X_2Bi_3)_q$ where p, q = ⟨1,2,3...⟩ and X = Se, Te, S. Most of the minerals from the tetradymite group correspond to the former type of structure whereas others, *e.g.*, poubaite and rucklidgeite represent a second type (assuming analogy with a synthetic Bi_3Se_4; $R\bar{3}m$; Z = 3; Semiletov & Pinsker, 1955).

Geological setting, occurrence and paragenesis

The Vihorlatské vrchy (Vihorlat Hills) represent a mountain range about 55 km long and 11 km wide. The western part of the range lies in the easternmost part of Slovakia and the smaller, eastern, part is located in Ukraine. The formation of a chain of calc-alkaline Neogene volcanics in this region is closely related to the development of the Eastern Slovakian Neogene Basin representing a part of the Transcarpathian Interarc Basin.

Vihorlatite was discovered in the area of the Morské Oko stratovolcano. The volcano is located over the intersection of NW – SE running, transversal, north-east striking faults with a NE – SW trending system of parallel faults. In the north and east, the Morské oko volcanic rocks overlie the Paleogene flysh sediments. The Neogene Molasse sedi-

DOI: 10.1127/0935-1221/2007/0019-1715
0935-1221/07/0019-1715 $ 4.95

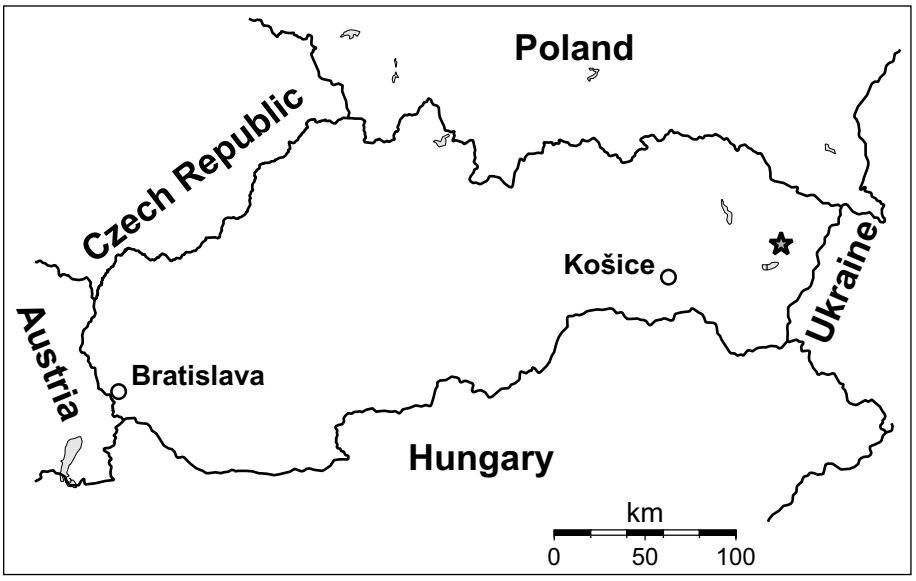

Fig. 1. Sketch map of Slovakia with the Vihorlat Mts. shown with a star.

ments are in contact with the base of the volcano in the south (Karpatian-Panonian sequences) and in the west (Eggenburgian sediments). In the SW, the Morské oko Stratovolcano rocks overlie the products of Sokolský potok and Vihorlat stratovolcanoes. On the SE side, the Morske oko Stratovolcano contacts the Diel Stratovolcano. Radiometric dating of the Morské oko volcanics provided ages between 12.4 and 9.4 Ma (Žec *et al.*, 1997).

The Morské oko Stratovolcano is composed of the Hámre and Sninský kameň Formations and the Central Volcanic Zone. The Hámre Formation is characterized by medium-porphyric pyroxenic lava flows and a discontinuous bed of redeposited tuffs. The formation builds up the base of the stratovolcano. The Sninský kameň Formation comprises a ring around the central zone. It discomformably overlies the moderately to strongly denudated surface of the Hámre Formation. The base of the formation is built up predominatly of coarse-porphyric pyroxenic andesite lava flows and the upper part comprises medium-fine-porphyric pyroxenic andesites, grading to basaltic andesites. The Central Volcanic Zone crops out in a cauldron-like depression on the slopes of the Morské oko and the Okna valleys. It consits of a series of volcanics and intrusives, frequently propylitized or chloritized. These rocks include andesitic porphyries and andesites, diorites and diorite porphyries, dykes and intrusions of pyroxenic andesite and andesite porphyry. In addition, bodies of secondary quartzites, silicified and argilitized zones are present in the central Volcanic Zone (Bacsó, 1986; Žec *et al.*, 1997). The Quaternary cover, consisting of loamy-stony, deluvial-fluvial, fluvial, eolian-deluvial, proluvial, solifluction and gravitational sediments, reflects the geological structure of pre-Quaternary basement (Žec *et al.*, 1997).

The vihorlatite-bearing bismuth-tellurium mineralization is bound to bodies of secondary quartzites of the Central Volcanic Zone cropping out in the Porubský Brook valley (Fig. 2). These quartzite bodies attains up to a few hundreds meters across. Massive grey to greenish quartzites are composed of quartz, opal, kaolinite, tridymite, and, in subordinate amount, boehmite, diaspore, topaz, andalusite, mullite, dumortierite, dickite, fluorite, zunyite, hematite and corundum. The Bi-Te-Se mineralization is related to magmatic and later hydrothermal and metasomatic activity of the Central Volcanic Zone. These later alterations also produced additional polymetallic Pb–Zn–Cu(+Ag+Au) mineralization characterized by occurrence of sphalerite, galena, cinnabar, chalcopyrite, pyrite, pyrrhotite, and small amounts of Ag and Au. Locally, also molybdenite, arsenopyrite, boulangerite, stannite and tetradymite occur (Bacsó & Ďuďa 1988). Gangue minerals in the latter mineralization are represented by quartz, calcite, dolomite, kaolinite, and less frequently also barite, cerussite, gypsum and zeolites (laumontite, chabazite, stilbite).

Table 1. Reflectance data (%) for vihorlatite measured in air with WTiC standard.

λ (nm)		R_{max}	R_{min}
420		50.7	48.1
440		51.7	49.2
460		52.8	49.8
470	**COM**	**52.9**	**49.9**
480		53.0	50.0
500		53.6	50.3
520		54.0	50.5
540		54.4	50.5
546	**COM**	**54.5**	**50.6**
560		54.7	50.9
580		54.6	51.0
589	**COM**	**54.6**	**51.0**
600		54.6	51.0
620		54.8	51.2
640		54.8	51.1
650	**COM**	**54.7**	**51.2**
660		54.6	51.2
680		54.6	51.0
700		54.6	50.9

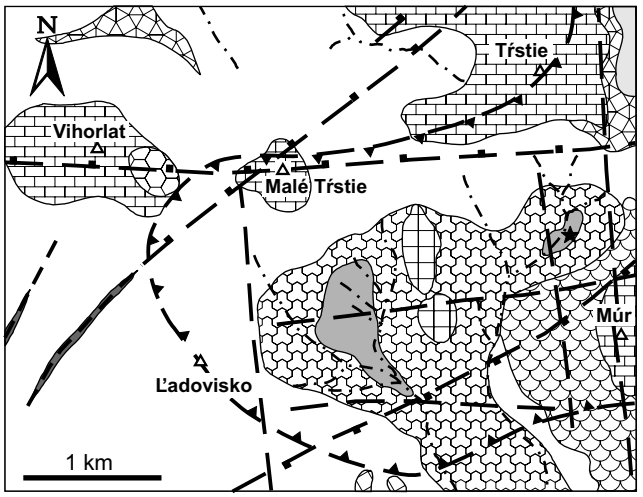

Lower Panonian magmatic stage:
extrusion-intrusion of porphyric pyroxene andesite
extrusions and short lava flows of pyroxene andesite
Upper Sarmatian magmatic stage:
secondary quartzites and Al-rich metasomatites
extrusion-intrusions of hornblende-pyroxene andesites
dike bodies of hornblende-pyroxene andesites
lava flow of pyroxene andesite
lapilli-pumice tuffs
lava flow of pyroxene andesite
Upper Badenian to Middle Sarmatian magmatic stage:
strongly hydrothermally altered pyroxene andesite of
volcano-tectonic depression
fault boundaries of volcano-tectonic depression
fault boundaries of local volcano-tectonic horst systems
fault lines
boundaries of geological units
watercourses
local summits
the place where vihorlatite was found

Fig. 2. Geological map of the part of the Morské oko Lake stratovolcano with a star indicating the place where vihorlatite occurs.

Samples containing vihorlatite come from the secondary quartzites. Vihorlatite occurs as disseminated grains or nests in quartz-opal veinlets a few millimeters thick or directly in secondary quartzites hosting these veinlets. In the closest association with vihorlatite only tetradymite, telluronevskite, opal, quartz, and microscopic grains of scheelite and stannite were found.

Physical and optical properties

Macroscopically, the aggregates of vihorlatite are steel-grey with metallic lustre and black streak, resembling tetradymite or tellurobismuthite. Vihorlatite forms anhedral grains or lamellar crystals 1–2 mm in size flattened parallel to (0001)

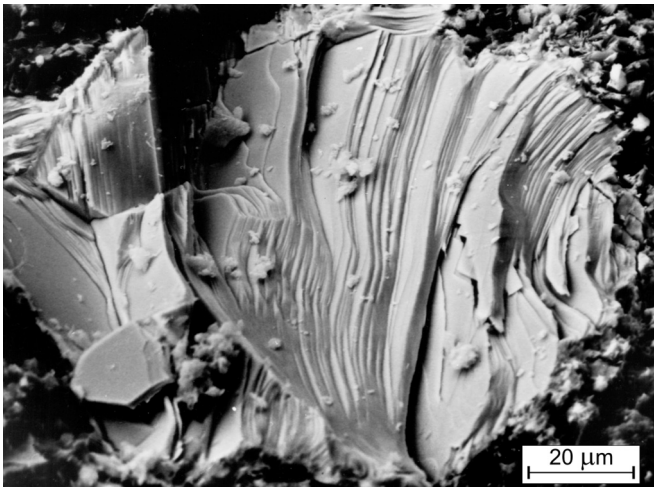

Fig. 3. Vihorlatite grain imaged in secondary electrons shows multiple (sub)parallel intergrowth and bending of individual platelets.

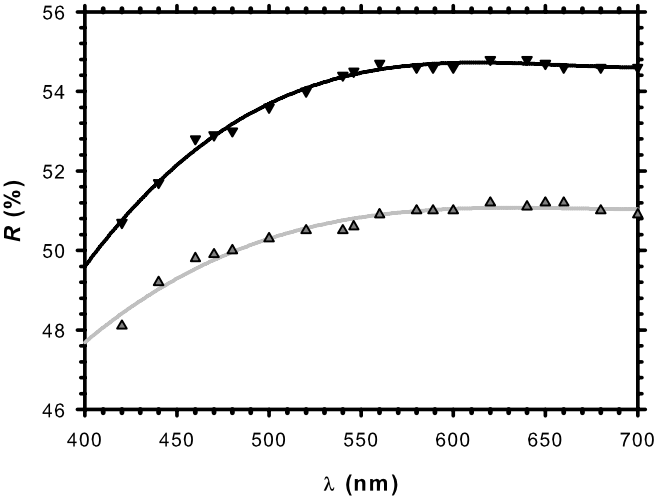

Fig. 4. Reflectance data for vihorlatite measured in air. Filled down-triangles correspond to R_{max} while gray up-triangles represent R_{min} values.

and aggregates thereof (Fig. 3). Rarely, also, individual grains reaching up to 8 mm in diameter occur. Vihorlatite crystals are frequently bent and display deformation lamellae in a polished section. Thin tabular crystals are flexible. When altered, vihorlatite becomes dull and darker and a red-brown rim appears on grain boundaries and along internal fractures. In reflected light, the colour is white with a yellowish tint. Bireflectance is weak, noticeable in oil and ranging from yellowish white to grey, but not perceptible in air. Anisotropy is moderate with grey to bluish grey polarization colours. No internal reflections were observed. Vihorlatite has a perfect cleavage parallel to (0001).

Reflectance values measured in air with a WTiC standard are given in Table 1 and plotted in Fig. 4. Vihorlatite reflectance curves are characterized by a steady increase of reflectance with increasing wavelength up to approximately 560 nm, after which the reflectance values remain invariant. The reflectance curves resemble those of, *e.g.*, tsumoite, sulphotsumoite, telluronevskite and ingodite (Chvileva *et al.*, 1988; Řídkošil *et al.*, 2001). The majority of minerals belonging to the tetradymite group displays slightly higher

overall reflectance compared to vihorlatite within the wavelength range studied.

Vickers microhardness measured with a 50 g load (VHN_{50}) is 65.9 kg/mm^2 (average of 30 indentations ranging from 49.2 to 91.7 kg/mm^2). A microhardness anisotropy was observed: ~55 kg/mm^2 in a section approximately perpendicular to [0001] and ~85 kg/mm^2 in a section approximately parallel to [000l]. According to published data (Chvileva *et al.*, 1988), vihorlatite is harder than tetradymite, joséite-B, laitakarite, and ingodite; its microhardness is close to sulphotsumoite, hedleyite, and ikunolite; and it is softer than tsumoite, telluronevskite, joséite-A, nevskite, or paraguanajuatite. A measured density of 8.0(2) g/cm^3 was obtained by weighing of 0.054 g of the mineral in toluene at room temperature.

Chemical composition

Several grains of vihorlatite were analyzed with a JEOL JCXA 733 WD electron microprobe at the Geological Survey of the Slovak Republic, Bratislava. Elements other than Bi, Se, Te, S, Au, Ag and Sb were not detected by preliminary qualitative analysis. The following operating conditions were used: accelerating voltage 20 kV; beam current 25 nA; analytical lines: Bi$M\alpha$, Se$L\alpha$, Te$L\alpha$, S$K\alpha$, Au$M\alpha$, Ag$L\alpha$, Sb$L\alpha$; standards: pure elements Bi, Sb, Au, Ag, Se, Te and galena (for S). Analytical results were corrected using the ZAF correction routine.

Three typical electron microprobe analyses and their average are given in Table 2. The empirical formula calculated on the basis of 45 atoms from the average chemical analysis, neglecting low contents of Sb, Au, and Ag, corresponds to $Bi_{21.9}Se_{17.4}Te_{4.1}S_{1.6}$. The idealized formula is $Bi_{24}Se_{17}Te_4$.

At the rims of the altered vihorlatite grains and along fractures within them, an alteration product occurs. Its composition was determined employing ED system (in wt. %) as Bi 62.6, Te 11.3, Se 7.1 and Fe 0.7, totalling 81.7 wt. %. Recalculation of that analysis leads to the empirical formula $Bi_3(TeO_6)(SeO_3)(OH) \cdot 3\ H_2O$.

Table 2. Typical and average chemical analyses of vihorlatite (in wt. %) and empirical formula based on 45 atoms per formula unit.

	1	2	3	4	5
Bi	72.48	71.10	71.00	71.5(8)	21.9(2)
Se	21.53	21.20	21.40	21.4(2)	17.4(2)
Te	8.04	7.85	8.41	8.1(3)	4.1(1)
S	0.73	1.19	0.59	0.8(3)	1.6(5)
Au	< 0.01	< 0.01	0.04	< 1 σ	< 1 σ
Ag	0.04	< 0.01	< 0.01	< 1 σ	< 1 σ
Sb	0.01	0.04	0.07	0.04(3)	0.02(1)
Total	102.83	101.38	101.51	101.9(9)	

1-3: typical electron microprobe analyses
4: average chemical composition
5: empirical formula calculated from the data in column 4

X-ray diffraction and crystal structure

Powder diffraction data were collected using a Philips X'Pert MPD Bragg-Brentano diffractometer (copper tube; 40 kV/40mA; graphite secondary monochromator). Three patterns were step-scanned (pattern #: range in °2θ; step size in °2θ; counting time in s.; #1: 11.0–149.99; 0.03; 61 / #2: 15.0–96.54; 0.02; 30 / #3: 1.5–80.0; 0.02; 30) with specimens prepared as slurry mounts on flat low-background silicon wafers.

Peak positions were obtained from the powder data by fitting with a program XFIT (Cheary & Coelho, 1992; Coelho & Cheary, 1998). The peaks below 65 °2θ were approximated with an asymmetric Pearson VII profile shape function and those above this limit with a symmetric pseudo-Voigt profile shape function. Refinement, next to the peak positions, produced also peak integral intensities and halfwidths. Diffraction maxima are broad (Fig. 5) which results in merging of possible close spaced reflections into clusters. This, makes separation of individual diffractions impossible which, in turn, introduces a bias in the refinement of the unit-cell dimensions.

To increase reliability and accuracy of the unit-cell parameters, they were refined from joint powder diffraction data. The parameters calculated by a least-square program (Burnham, 1962) from totally 160 indexed diffraction lines and applying the $\cos\theta\cot g\theta/\lambda^2$ correction term are: a = 4.2797(9) Å, c = 87.01(2) Å, c/a = 20.332(6), V = 1380.2(6) Å^3. For Z = 1 the calculated density is D_x = 7.850(3) g/cm^3. Indexing of the powder pattern (Table 3) was based mainly on the data obtained from the precession photographs (see below).

Single-crystal study was carried out with a precession camera. Many of the tested crystals, however, were found unsuitable for single-crystal study because they often displayed subparallel intergrowths and/or heavy crystal bending (see also Fig. 3). These defects resulted in extreme radial streaking of diffraction spots. Nevertheless, finally, one tabular fragment showing relatively slight reflection streaking only, which was limited mostly to reflections in *h0l* reciprocal lattice, was found. The effect of the radial streaking is

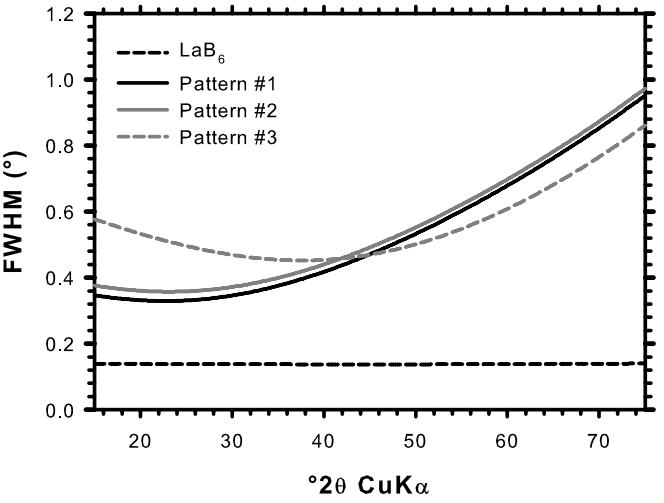

Fig. 5. Peak halfwidths measured in individual powder patterns of vihorlatite compared to those of LaB_6 standard. Considerable peak broadening leads to overlap of closely spaced reflections.

Table 3. Powder X-ray diffraction data for vihorlatite.

h	k	ℓ	$2\theta_{obs}$	$2\theta_{obs,c}$	$d_{obs,c}$	d_{calc}	I_{obs}	I_{calc}
0	0	12	12.13	12.20	7.25	7.25	8.3	2.6
0	0	19	19.43	19.47	4.55	4.58	55.4	4.9
0	1	4	24.40	24.43	3.640	3.653	11.1	10.6
1	0	8	25.38	25.41	3.502	3.508	2.7	2.2
0	1	11	26.68	26.71	3.335	3.356	15.1	7.5
0	0	26				3.346		1.5
1	0	15	28.60	28.63	3.116	3.123	100.0	100.0
1	0	22	33.18	33.20	2.696	2.704	3.0	0.8
0	1	23	33.76	33.78	2.651	2.647	9.3	1.9
1	0	27	36.89	36.91	2.433	2.432	2.5	0.6
0	1	30	39.43	39.45	2.282	2.284	75.5	24.0
1	1	0	42.21	42.23	2.138	2.139	26.4	39.1
1	0	34	42.88	42.90	2.107	2.106	14.2	1.1
0	1	37	45.73	45.75	1.982	1.985	2.4	0.3
1	1	19	46.93	46.95	1.934	1.938	42.8	3.1
0	0	45				1.933		1.8
1	0	41	49.53	49.54	1.838	1.841	6.2	1.7
2	0	4				1.846		0.6
0	1	42				1.808		0.1
2	0	11	50.43	50.45	1.808	1.804	3.5	1.4
1	1	26				1.803		1.8
0	2	15	51.67	51.69	1.767	1.765	31.5	17.4
0	0	52	54.91	54.92	1.670	1.673	6.2	0.1
2	0	23				1.664		0.4
0	1	49	57.44	57.45	1.603	1.601	10.6	0.1
2	0	30	59.06	59.07	1.5626	1.5614	17.8	0.6
1	1	38				1.5632		6.6
1	0	52	60.47	60.48	1.5294	1.5248	1.1	0.5
0	2	34	61.66	61.67	1.5028	1.5007	3.5	0.4
1	0	53				1.5008		0.1
1	1	45	64.87	64.88	1.4360	1.4344	25.6	3.7
2	1	15	68.85	68.86	1.3624	1.3615	11.6	13.3
1	0	60	69.53	69.53	1.3508	1.3503	9.2	0.3
1	1	52	71.54	71.55	1.3177	1.3179	2.0	0.1
1	2	23				1.3135		0.4
2	0	49	73.78	73.79	1.2831	1.2819	1.5	0.1
1	2	30	75.20	75.20	1.2624	1.2612	10.0	5.9
1	1	57	76.47	76.48	1.2445	1.2425	1.4	0.1
3	0	0	77.28	77.29	1.2335	1.2352	4.8	5.4
2	1	34	77.76	77.76	1.2271	1.2286	2.0	0.3
1	0	67	77.90	77.90	1.2253	1.2254	2.5	0.1
3	0	19	80.39	80.40	1.1934	1.1926	0.7	0.1
1	1	64	84.12	84.13	1.1498	1.1474	7.4	0.1
0	2	60	84.63	84.63	1.1442	1.1419	3.5	0.2
0	1	75	88.19	88.20	1.1069	1.1070	2.5	0.1
2	2	0	92.20	92.21	1.0690	1.0697	2.0	3.3
1	1	71	92.97	92.97	1.0621	1.0633	1.9	0.1
1	0	79	93.72	93.73	1.0556	1.0556	2.1	0.1
0	3	45	95.30	95.30	1.0422	1.0409	2.8	0.4
2	2	19				1.0417		0.6
0	1	82	98.16	98.17	1.0194	1.0200	2.0	0.1
1	1	75				1.0197		0.1
3	1	11				1.0192		0.1
2	2	26				1.0189		0.5
1	3	15	98.93	98.93	1.0135	1.0120	1.6	4.8
2	1	60	99.68	99.69	1.0078	1.0074	3.2	0.2
2	0	75	103.27	103.28	0.98237	0.98319	1.6	0.1
3	1	30	105.34	105.34	0.96869	0.96872	4.1	0.1
2	2	38				0.96916		2.6
2	1	67	107.99	108.00	0.95214	0.95223	1.9	0.2
1	3	34				0.95371		0.1
1	2	68	109.17	109.18	0.94513	0.94462	0.9	0.1
2	1	69	110.39	110.40	0.93807	0.93708	1.1	0.1
1	3	41	112.97	112.97	0.92388	0.92497	2.1	0.1
4	0	15	114.48	114.48	0.91596	0.91482	4.4	2.0
0	1	94	118.12	118.13	0.89804	0.89793	1.2	0.1
1	2	75	119.44	119.45	0.89194	0.89337	2.8	0.1
0	4	30	121.81	121.81	0.88151	0.88248	3.2	1.6
1	1	90				0.88091		0.1
2	1	79	125.85	125.85	0.86508	0.86570	0.7	0.1

Table contains measured angular data ($2\theta_{obs}$); angular data corrected with the correction term ($2\theta_{obs,c}$); d-spacings calculated from corrected angular data ($d_{obs,c}$); d-spacings calculated from the refined unit cell dimensions in the last cycle of refinement (d_{calc}); measured intensities (I_{obs}); and those calculated from the crystal structure (I_{calc}). The angular data given were obtained as an average of those from individual patterns employed in the joint unit-cell refinement.

Unit-cell from joint refinement of the 3 combined powder patterns:

λ= 1.54056 Å

a = 4.2797(9) Å

c = 87.01(2) Å

V = 1380.2(6) Å^3

c/a = 20.332(6)

N = 160

M = 152

λ – wavelength used to convert angular data to d-spacings; N – number of diffraction indices in the first cycle of refinement; M – number of diffraction indices in the last cycle of refinement.

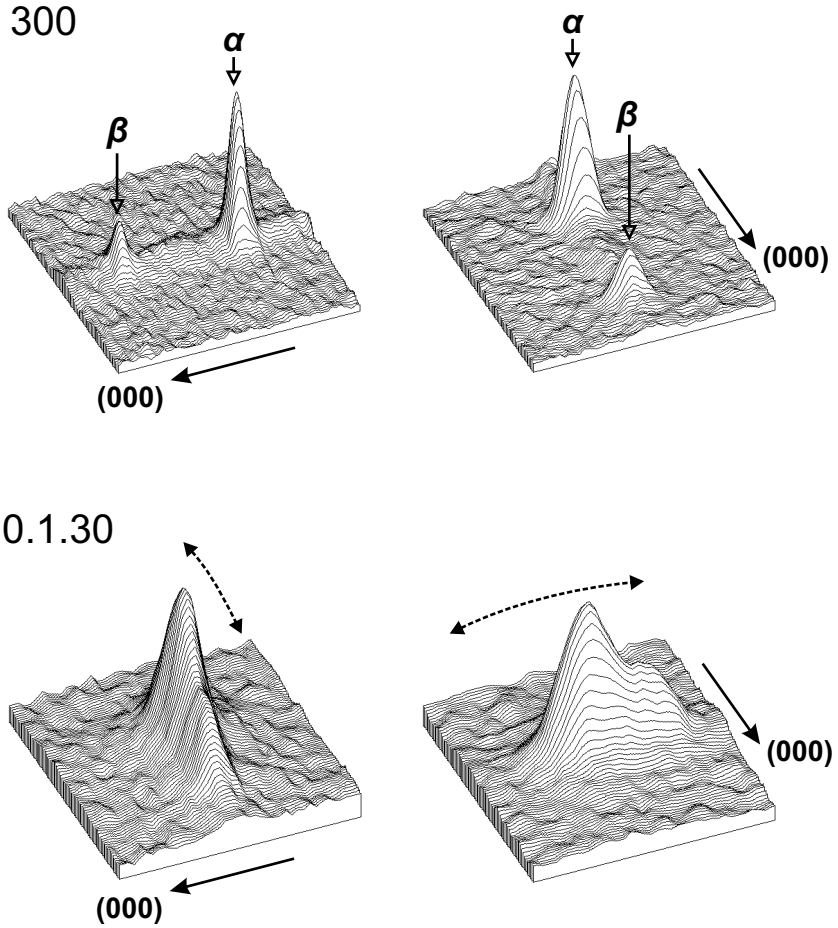

Fig. 6. Three-dimensional intensity distribution for 300 and 0.1.30 reflections demonstrating the radial streaking of *h*0*l* reflections. The 0.1.30 reflection is significantly smeared, whereas the 300 one has almost isometric shape. It is due to crystal bending and sub-parallel intergrowths of individual platy crystals forming the studied grain.

shown in Fig. 6 where a 3D-profile of the reflection 0.1.30 is compared to an unaffected diffraction spot 300. Still, the quality of that crystal was not high enough to allow reliable data collection with a four-circle diffractometer.

The precession photographs were taken using Zr-filtered Mo*K* (*hk*0, *h*0*l*, and *hhl* reciprocal lattices), unfiltered Mo*K* (*hk*0 reciprocal lattice) and Ni-filtered Cu*K* (*h*0*l* reciprocal lattice) radiations. The precession angle was $\overline{\mu} = 25°$. Orientation photographs ($\overline{\mu} = 10°$, **c**-axis) taken with unfiltered Mo*K* radiation and without a layer-line screen revealed trigonal symmetry though *hk*0 reciprocal lattice has *p* 6*mm* plane symmetry. The trigonal symmetry was proved also by cone-axis photograph taken along **c**. Symmetry of *h*0*l* and *hhl* reciprocal planes corresponds to *p* 2 and *p* 2*mm* plane groups, respectively, and of cone-axis ***c*** photograph has *p* 3*m*1 plane symmetry. These observations result in the $\overline{3}m$ Laue class. The lack of systematic absences indicates $P\overline{3}m$l, *P*321 and *P*3*m*1 as possible space groups. Most of the minerals within the tetradymite group and synthetic trigonal bismuth chalcogenides which does not show *R*-lattice centering crystallize in $P\overline{3}$ml space group (Bayliss, 1991; Stasova, 1967). Consequently, we adopted this symmetry for our further structure considerations. Unit-cell parameters calculated from precession recordings applying the procedure of Rieder (1973) are $a = 4.29(2)$ Å, $c = 86.7(2)$ Å, $V = 1383(14)$ Å^3. The size of the unit-cell parameter c is substantiated also by the results of the cone-axis study ($c = 87.6(4)$ Å using the extrapolation procedure of Quarashi & Barnes, 1953).

In general, trigonal layered bismuth chalcogenides display crystal structures consisting of individual atomic layers: *A* (0; 0; z_A), *B* (1/3; 2/3; z_B), and *C* (2/3 ;1/3; z_C). These are stacked along the **c**-axis with overall sequence *ACB* (Abrikosov & Stasova, 1985; Stasova, 1967). The layers are usually arranged to Bi–Bi double-layer sheets (or alternatively X-X) and X–Bi–X–Bi–X five-layer sheets (or alternatively Bi-X-Bi-X-Bi) where X stands for chalcogenic elements Se, Te or S. For the purpose of this paper the double-layer Bi-Bi sheets are called T and five-layer X-Bi-X-Bi-X sheets are named U. The unit-cell parameters of these phases are generally: $a \sim 4.2 - 4.3$ Å and $c \sim (1.94 \cdot N)$ Å where N corresponds to the number of atomic layers within the unit cell (Strunz, 1963). Simultaneously, it holds that $N = Z \cdot (p + q)$ where Z is the number of formula units within the unit cell and p, q are indices of a chemical formula Bi_pX_q (Stasova & Karpinskii, 1967). Chemical formulae and the number of individual structural layers are thus tightly coupled with the length of the unit-cell parameter c.

Since the unit cell parameter *c* of vihorlatite attains ~ 87 Å a structure model with 45 atomic layers is to be found. The crystal structure of vihorlatite is best explained with that of Bi_8Se_7 archetype (Stasova, 1967) though this model requires a substantial Se ↔ Bi substitution. Using the sheet nomenclature introduced above and the numbering of the sheets, the unit cell content of Bi_8Se_7 may be described as

$$^1U - {}^1T - {}^2U - {}^3U - {}^2T - {}^4U - {}^3T - {}^5U - {}^4T - {}^6U - {}^7U - {}^5T - {}^1U$$

where italicized symbols indicate that only a half of a corresponding structure block is present in the unit cell. Since ^3T double-layer halves the unit cell, the sheets ^5U, ^6U, ^7U, ^4T, and ^5T represent symmetrical equivalents of the sheets left of the ^3T shown in the diagram above. Overall formula using the same symbolism can be given as T_5U_7. Existence of the structural archetype allowed to develop the initial structure model as well as to significantly constrain the subsequent structure refinement.

Comparison of visually estimated intensities of reflections in precession photographs with those calculated [with FullProf by Rodríguez-Carvajal (1990, 2005)] from an initial structure model assuming a statistical distribution of Te atoms over sites occupied by Se revealed that certain discrepancies exist in intensity distribution between the observed and calculated data, particularly for *h*0*l* reflections. To elucidate the possible ordering in the crystal structure of vihorlatite, individual reciprocal rows in the the precession recordings taken were scanned with a flatbed scanner. Scans were converted to X-Y-pairs with a program ImageJ (Abramoff *et al.*, 2004) following the modified procedure of Palmer (1997). Subsequently, these files were loaded to a program WinPlotr (Roisnel & Rodriguez-Carvajal, 2001) where background was manually subtracted and data smoothed – an example of 10*l* reciprocal row is shown in Fig. 7. Reflection intensities were measured in such modified scans using approximation with a symmetrical pseudo-Voigt function. Then, intensities from different reciprocal lattices were scaled based on common or symmetrically equivalent reflection(s). After scaling, the intensities were corrected with a combined Lorenz-polarization factor taken from Lipson (1967). An absorption correction was neglected since the impact on the quality of the data would be questionable because of irregular crystal shape.

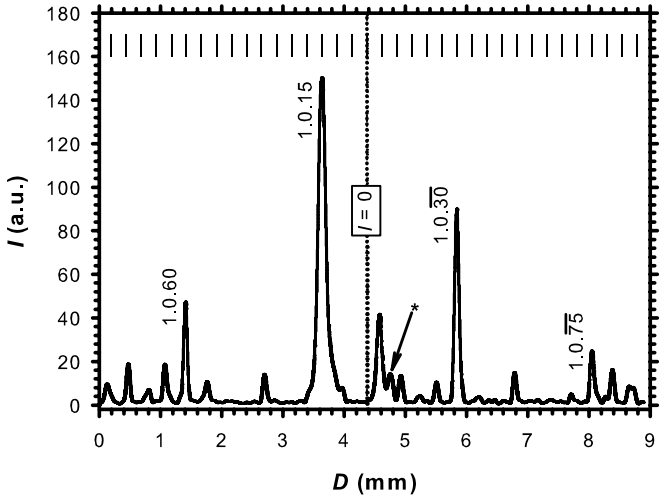

Fig. 7. Smoothed scan of 10*l* reciprocal row recorded with Zr-filtered Mo*K* radiation with a precession camera. Diffraction indices are shown for the most intense reflections. Tick marks at the top of the graph correspond to $l = 5n$. An asterisk shows the peak due to a streak of general radiation pointing to $2.0.\overline{15}$ reflection.

Several structure models based on Bi_8Se_7 archetype were developed in the following step to reflect possible ordering schemes of chalcogenic atoms within the structure. Squared structure factors calculated from these structure models using a program FullProf (Rodríguez-Carvajal, 2005) were corrected with the Lorentz-polarization factor for precession method and compared to those obtained from precession recordings. This comparison showed that Te atoms are ordered in the structure and they are located on the neighbouring margins of ^2U and ^3U (and symmetrically equivalent ^6U and ^7U) five-layer sheets. As a result Te-Te double-layers form in the crystal structure of this mineral. Using the symbol U' for a Te-substituted U-sheet with the apostrophe indicating the placement of Te atom in such structure block the crystal structure of vihorlatite can be written as

$$U - T - U' - 'U - T - U - T - U - T - U' - 'U - T - U$$

resulting in the overall formula $T_5U_3U'_4$ or $(Bi_2)_5(Bi_2Se_3)_3(Bi_2Se_2Te)_4$ giving the idealized chemical formula of vihorlatite $Bi_{24}Se_{17}Te_4$. It should be noted that Te-double layers identical to those in vihorlatite are present in telluronevskite (Řídkošil *et al.*, 2001) and similar type of Te-double layers can be found in tetradymite (Harker, 1934) or kawazulite (Bland & Basinski, 1961). Symbolic formula of telluronevskite is TU'_2 where U' = Se – Bi – Se – Bi – Te. The symbolic formulae of tetradymite and kawazulite are $'U'_3$ with U = Te – Bi – S – Bi – Te and Te – Bi – Se – Bi – Te, respectively.

Considering the actual chemical composition (Table 2), results of structure modelling, and assuming substitution schemes reported commonly from other minerals of the tetradymite group (Bayliss, 1991), the empirical formula of vihorlatite reflecting the crystal structure becomes $[(Bi_{0.99}Te_{0.01})_2]_5[(Bi_{0.86}Se_{0.14})_2(Se_{0.9}S_{0.1})_2Te]_4[(Bi_{0.86}Se_{0.14})_2(Se_{0.9}S_{0.1})_3]_3$. This corresponds to the substitutions Se ↔ Bi amounting approximately 14 at. % and that of Se ↔ S attaining about 10 at. %.

Having an appropriate crystal structure model and fixing the element substitutions as described above, the structure refinement was carried out with a program FullProf (Rodríguez-Carvajal, 2005). The refinement was performed jointly against two powder patters: No. 1 and No. 2 mentioned above. Remaining pattern was excluded from the structure refinement because of poor counting statistics compared to those two involved in the refinement. Weights given to each of the two patterns were manually varied to provide the best overall fit – finally, a proportion 0.6 to 0.4 was chosen which also roughly corresponded to the angular range covered by individual patterns. In the initial stages of the refinement the unit-cell parameters were adopted from the LeBail fitting (they matched those refined from indexed individual diffraction maxima within 2σ range) and kept constant; they were allowed to vary in the last stages of the

refinement. Varied structural parameters included *z*-fractional atomic coordinates, multiaxial March-Dollase preferred orientation parameters and isotropic temperature factors. The powder pattern specific parameters refined comprised profile half-widths and shape values, and microabsorption (sample roughness) and cosine sample displacement corrections. The fractional *z*-coordinates were hard-constrained using the interatomic distances computed from structure data of Bi-Te-Se-S phases and minerals listed in the ICSD database (2003). The microabsorption correction parameters were also hard-constrained to provide mathematically reasonable values. The temperature factors were allowed to vary jointly for groups of identically occupied atomic sites. These constraints and restraints and the use of two individual patterns allowed fitting crystal structure even from the relatively low-resolution X-ray powder diffraction data (Fig. 5). Details on the structure refinement are summarized in Table 4. Resulting atomic coordinates and selected inter-atomic distances are given in Tables 5 and 6, respectively. The structure is shown in Fig. 8. Validity of the crystal structure was confirmed also independently using the precession data. Intensities generated from the crystal structure refined from powder patterns match fairly those observed in precession photographs.

Mineral relationships

Vihorlatite is a member of the tetradymite group. Originally, Strunz (1982) defined this group (as "tetradymite-ikunolite-paraguanajuatite group") to include hexagonal (mostly rhombohedral) minerals and synthetic compounds of $(Bi, Pb)_x(Te,Se,S)_y$ composition and unit cell dimensions $a \sim 4.2$ Å and $c \sim 3n \times 1.95$ Å. He subdivided the group into 3 series with $n = 3$ (tetradymite series), $n = 7$ (ikunolite series), and $n = 9$ and 20 (paraguanajuatite and hedleyite, respectively). Later, this definition was revisited and widened by Bayliss (1991). In his approach, next to the minerals incorporated already by Strunz, the group included elemental Se, Te (tellurium subgroup), Sb, As, Bi and stibarsen (arsenic subgroup) and also minerals containing Ag and Sb. Bayliss (1991) defined eight subgroups within the tetradymite group based on the number of atomic layers perpendicular to **c** in the same way as Strunz (1982) did. Most recently,

Table 4. Material data, data acquisition and structure refinement details for vihorlatite.

Material data		
Empirical formula	$Bi_{21.9}Se_{17.3}Te_{4.1}S_{1.7}$	
Formula weight	6525.4	
Crystal system, space group	trigonal, $P\bar{3}m1$ (164)	
Unit-cell dimensions , a (Å)	4.277(1)	
, c (Å)	86.93(2)	
, V (Å^3)	1376.9(6)	
Z	1	
D_x (g.cm^{-3})	7.869(3)	
Data collection		
Diffractometer	Philips X'Pert MPD	
Geometry	reflecting θ-2θ Bragg-Brentano	
Monochromator	secondary curved graphite	
Sample	powder slurry mount, low-background holder	
Wavelengths (Å)	1.54056 & 1.54433	
Joint refinement:	Pattern #1	Pattern #2
Weight	0.6	0.4
Angular range / step (°)	11.00 – 130.00 / 0.03	15.00 – 96.54 / 0.02
Reflections	1483	832
Refinement:		
Program package	FullProf	
Profile shape function	pseudo-Voigt	
Corrections	multi-dimensional March-Dollase microabsorption (sample roughness) sample displacement (cosine term)	
Parameters	56	
Constraints	34	
Restraints	4	
R_p	3.37	5.80
R_{wp}	4.73	7.62
R_{exp}	4.05	7.82
χ^2	1.36	0.94
R_B	9.11	8.40
R_F	6.44	4.88
Global user-weighed χ^2	1.19	

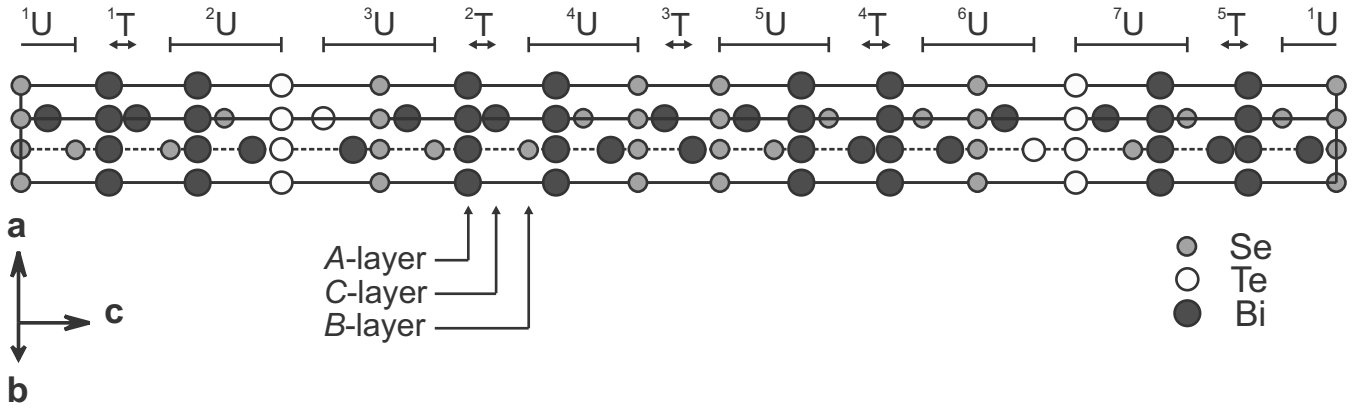

Fig. 8. Crystal structure of vihorlatite consists of double-layer sheets (T) and five-layer sheets (U). The five-layer sheets ^{2}U, ^{3}U, ^{6}U and ^{7}U display ordered Se ↔ Te substitution. These blocks showing Te ordering with halves of adjacent T sheets correspond to telluronevskite stakking sequence.

Table 5. Atomic coordinates and isotropic displacement parameters (in Å^2) for vihorlatite.

Sheet	Atom type	Wyck.	Atomic occupancy	*x/a*	*y/b*	*z/c*	U_{iso}
1U	X1	1*a*	1	0.0	0.0	0.0000	0.027(7)
	Bi1	2*d*	2	2/3	1/3	0.0202(6)	0.015(3)
	X2	2*d*	1	1/3	2/3	0.0409(8)	0.027(7)
1T	Bi2	2*c*	3	0.0	0.0	0.0660(6)	0.012(3)
	Bi3	2*d*	3	2/3	1/3	0.0872(6)	0.012(3)
2U	X3	2*d*	1	1/3	2/3	0.1121(9)	0.027(7)
	Bi4	2*c*	2	0.0	0.0	0.1327(5)	0.015(3)
	X4	2*d*	1	2/3	1/3	0.1536(7)	0.027(7)
	Bi5	2*d*	2	1/3	2/3	0.1737(5)	0.015(3)
	X5	2*c*	4	0.0	0.0	0.1959(7)	0.023(8)
3U	X6	2*d*	4	2/3	1/3	0.2275(9)	0.023(8)
	Bi6	2*d*	2	1/3	2/3	0.2502(5)	0.015(3)
	X7	2*c*	1	0.0	0.0	0.2706(7)	0.027(7)
	Bi7	2*d*	2	2/3	1/3	0.2905(5)	0.015(3)
	X8	2*d*	1	1/3	2/3	0.3110(7)	0.027(7)
2T	Bi8	2*c*	3	0.0	0.0	0.3362(5)	0.012(3)
	Bi9	2*d*	3	2/3	1/3	0.3577(4)	0.012(3)
4U	X9	2*d*	1	1/3	2/3	0.3825(9)	0.027(7)
	Bi10	2*c*	2	0.0	0.0	0.4023(4)	0.015(3)
	X10	2*d*	1	2/3	1/3	0.4236(8)	0.027(7)
	Bi11	2*d*	2	1/3	2/3	0.4444(5)	0.015(3)
	X11	2*c*	1	0.0	0.0	0.4641(9)	0.027(7)
3T	Bi12	2*d*	3	2/3	1/3	0.4895(5)	0.012(3)

Atomic occupancies:
1: Se0.9S0.1
2: Bi0.86Te0.14
3: Bi0.99Te0.01
4: Te
The standard uncertainties given are corrected for correlated residuals.

Strunz & Nickel (2001) divided the tetradymite group into 5 subgroups with parameter *c* ranging from ~ 3 × 6 Å to ~ 12 × 6 Å, and chemical formula corresponding to M:(Te,S) 2:1, 1:1, to 2:3, 4:3, 3:4, *etc*. The length of 6 Å (or 3 × 1.95 Å) corresponds to a thickness of atomic stacks containing three single-atomic planes of BiX_2 or Bi_2X composition perpendicular to [0001]. In any of these three classification schemes, vihorlatite constitutes a new subgroup which is characterized with the number of layers *n* equal to 15 and M:(Se,Te,S) 8:7. It may be interpreted as an *ordered* accretional homologue consisting of two telluronevskite structure blocks (Bi-Bi_2Se_2Te, stacking sequence TU'ʻU, $N = 12$) interlaced by alternating single-TU (Bi-Bi_2Se_3-Bi, $N = 7$) and double-TU blocks (Bi-Bi_2Se_3-Bi_2-Bi_2Se_3-Bi, $N = 14$), respectively.

Table 6. Selected interatomic distances for vihorlatite.

Atom 1	Atom 2	Distance
Bi2	Bi3	3.08(4)
Bi8	Bi9	3.10(3)
Bi12	Bi12$^{\#}$	3.07(4)
Bi1	X1	3.03(3)
Bi1	X2	3.06(5)
Bi2	X2	3.30(6)
Bi3	X3	3.28(6)
Bi4	X3	3.05(5)
Bi4	X4	3.07(4)
Bi5	X4	3.03(4)
Bi5	X5	3.13(5)
Bi6	X6	3.16(6)
Bi6	X7	3.04(4)
Bi7	X7	3.02(4)
Bi7	X8	3.05(4)
Bi8	X8	3.30(5)
Bi9	X9	3.28(6)
Bi10	X9	3.01(5)
Bi10	X10	3.09(5)
Bi11	X10	3.06(5)
Bi11	X11	3.01(5)
Bi12	X11	3.31(6)
X5	X6	3.69(7)

Conclusions

Vihorlatite represents an ordered mineral with ordering of Te atoms identical to that found in telluronevskite. This type of ordering is most probably favoured by equilibrium hydrothermal conditions during mineral formation. The ordering also suggests that the process of crystallization from hydrothermal solutions was long enough to allow the crystallization of such ordered structures (expected temperature of these solutions was below 250 °C). Vihorlatite corresponds to an ordered accretional homologue derived from an archetypal crystal structure of Se-rich isomorphic phase Bi_8Se_7 reported by Stasova (1965) and is a member of the tetradymite group constituting its own subgroup. Natural counterparts of synthetic phases Bi_8Se_7 and Bi_8Te_7,which might be found in the future, would also belong to this subgroup.

Acknowledgements: Invaluable help of Yves Moëlo who discussed various aspects of the crystal structure model is sincerely acknowledged. In addition, the manuscript benefited from in-depth reviews by Luca Bindi and Nigel J. Cook. This study falls within the Institute of Geology AS CR research plan AV0 Z30130516.

References

Abramoff, M.D., Magelhaes, P.J., Ram, S.J. (2004) Image Processing with ImageJ. *Biophotonics Int.*, **11(7)**, 36–42,.

Abrikosov, N. Kh. & Stasova, M. M. (1985): Solid solutions based on bismuth and antimony tellurides and bismuth selenides. *Neorgan. Materialy*, **21**, 2011–2015. (In Russian).

Bacsó, Z. (1986): Geological formations and fault systems of stratovolcanoes of Vihorlat Mts. *Mineral. Slovaca*, **18**, 97–120. (In Slovak).

Bacsó, Z. & Ďuďa, R. (1988): Metallogenesis and ore formations of the Remetské Hámre ore field. *Mineral. Slovaca*, **20**, 193–220. (In Slovak).

Bayliss, P. (1991): Crystal chemistry and crystallography of some minerals in the tetradymite group. *American Mineral.*, **76**, 257–265.

Bland, J.A. & Basinski, S.J. (1961): The crystal structure of Bi_2Te_2Se. *Canad. J. Physics*, **39**,1040–1043.

Burnham, C.W. (1962): Lattice constant refinement. Carnegie Institution of Washington, Year Book, **61**, 132–135.

Cheary, R.W. & Coelho, A.A. (1992): A fundamental parameters approach to X-ray line-profile fitting. *J. Appl. Cryst.*, **25**, 109–121.

Chvileva, T.N., Bezsmertnaya M.S., Spiridonov, E.M., Agroskin, A.S., Papayan, G.V., Vinogradova, R.A., Lebedeva, S.I., Zavyalov, E.N., Filimonova, A.A., Petrov, K.K., Rautian, L.P., Sveshnikova, O.L. (1988): Handbook for determination of ore minerals in reflected light. Nedra, Moscow, 504 p. (In Russian).

Coelho, A.A. & Cheary, R.W. (1998): X-ray Line Profile Fitting Program, XFIT. A computer program. School of Physical Sciences, University of Technology, Sydney, Australia.

Ďud'a, R. (1985): Mineralogical and paragenetic relationships of ore mineralisation in the area of Remetské Hámre. *in* Z. Bacsó, ed., "Remetské Hámre – Final report and calculation of reserves. Hg-ores". Unpublished report, Geofond, Bratislava (In Slovak).

Harker, D. (1934) The crystal structure of the mineral tetradymite, Bi_2Te_2S. *Zeit. Kristall.*, **89**, 175–181.

ICSD (2003): Inorganic Crystal Structure Database (ICSD), Release 2003. – Fachinformationszentrum Karlsruhe (FIZ) and the National Institute of Standards and Technology (NIST).

Lipson, H. (1967): Physics of diffraction methods. *in* J.S. Kasper & K. Lonsdale, eds., "International Tables for X-ray Crystallography, Volume II, 2nd edition", The Kynoch Press, Birmingham, England, 235–315.

Palmer, D.C. (1997): Digital analysis of X-ray films. *Mineral. Mag.*, **61**, 453–461.

Quarashi, M.M. & Barnes, W.H. (1953): A note on cone-axis and upper level precession photographs. *Amer. Mineral.*, **38**, 552–556.

Řídkošil, T., Skála, R., Johan, Z., Šrein, V. (2001): Telluronevskite, Bi_3TeSe_2, a new mineral. *Eur. J. Mineral.*, **13**, 177–185.

Rieder, M. (1973): Precession photography: an extrapolation method for more accurate cell dimensions. *Acta Cryst.*, **A29**, 579–580.

Rodríguez-Carvajal, J. (1990): FULLPROF: A Program for Rietveld Refinement and Pattern Matching Analysis. *in* "Abstracts of the Satellite Meeting on Powder Diffraction of the XV Congress of the IUCr", Toulouse, France, 127 p.

– (2005): FullProf.2k. – Rietveld, Profile Matching and Integrated Intensity Refinement of X-ray and/or Neutron Data. Version 3.50, November 2005. A computer program. LLB, CEA-CNRS, Saclay, France.

Roisnel, T. & Rodríguez-Carvajal, J. (2001): WinPLOTR: a Windows tool for powder diffraction patterns analysis. *Materials Science Forum, Proceedings of the European Powder Diffraction Conference (EPDIC7)*, **378–381**, 118–123.

Semiletov, S.A. & Pinsker, Z.G. (1955): The electron diffraction analysis of the system of alloys Bi-Se. *Dokl. AN SSSR*, **100**, 1079–1082.

Sopková, A. (1977): Study of inclusions in topaz of secondary quartzites from the Vihorlat Mts. Unpublished Ph.D. thesis, Faculty of Science, Charles University, Prague. (In Slovak).

Stasova, M.M. (1965): X-ray diffraction study of homogeneity in the system bismuth-selenium. *Izvestiya AN SSSR, Neorganicheskie materialy*, **I(12)**, 2134–2137. (In Russian).

– (1967): The crystal structure of bismuth selenides and bismuth and antimony tellurides. *Zhournal Strukt. Khim.*, **8**, 655–660. (In Russian).

Stasova, M.M. & Karpinskii, O.G. (1967): About layering in structure of bismuth selenides and tellurides and antimony tellurides. *Zhurnal Strukt. Khim.*, **8**, 85–88. (In Russian).

Strunz, H. (1963): Homöotypie Bi_2Se_2–Bi_2Se_3–Bi_3Se_4–Bi_4Se_5 usw. (Platynit, Ikunolit, Laitakarit). *Neues Jahrb. Mineral. Monatsh.*, **1963**,154–157.

– (1982): Mineralogische Tabellen. 8. Auflage. Akademische Verlagsgeselschaft Geest & Portig K.-G., Leipzig. 621 p.

Strunz, H. & Nickel, E.H. (2001): Strunz mineralogical tables. Chemical-structural mineral classification system. 9th edition. Schweizerbart, Stuttgart, 870 p.

Žec, B., Kaličiak, M., Konečný, V., Lexa, J., Jacko, S., Jr., Baňacký, V., Karoli, S., Potfaj, M., Rakús, M., Petro,Ľ., Spišák, Z., Bodnár, J., Jetel, J., Boorová, D., Zlinská, A. (1997): Explanations to geologic map of Vihorlatské and Humenské vrchy Mts., scale 1: 50000. Geological Survey of the Slovak Republic, Bratislava, 254 p. (In Slovak).

Received 31 July 2006
Modified version received 10 November 2006
Accepted 18 December 2006